ENERGY CONFINEMENT AND MHD ACTIVITY IN SHAPED TCV PLASMAS WITH LOCALISED ELECTRON CYCLOTRON HEATING

A. POCHELON, S. ALBERTI, C. ANGIONI, S. BARRY, R. BEHN, P. BLANCHARD, P. BOSSHARD, R. CHAVAN, S. CODA, B.P. DUVAL, D. FASEL, A. FAVRE, S. FRANKE, I. FURNO, T.P. GOODMAN, P. GORGERAT, M. HENDERSON, F. HOFMANN, J-P. HOGGE, P-F. ISOZ, B. JOYE, J.B. LISTER, X. LLOBET, J-C. MAGNIN, P. MANDRIN, A. MANINI, B. MARLETAZ, Ph. MARMILLOD, Y. MARTIN, J-M. MAYOR, J-M. MORET, Ch. NIESWAND, P.J. PARIS, A. PEREZ, Z.A. PIETRZYK, R.A. PITTS, A. REFKE, H. REIMERDES, J. ROMMERS, O. SAUTER, W. VAN TOLEDO, G. TONETTI, M.Q. TRAN, F. TROYON, P. VYAS, H. WEISEN
Centre de Recherches en Physique des Plasmas,
Association EURATOM - Confédération Suisse
Ecole Polytechnique Fédérale de Lausanne
CH-1015 Lausanne, Switzerland

Y.V. ESIPCHUCK, N. KIRNEVA, A.A. MARTYNOV, K.A. RAZUMOVA, A. SUSHKOV
Institute of Nuclear Fusion, Russian Research Centre,
Kurchatov Institute
123 182 Moscow, Russia

F. PORCELLI, E. ROSSI
Dipartimento Di Energetica
Politecnico di Torino
I-10129 Torino, Italy

Abstract

Confinement in TCV (Tokamak à Configuration Variable) EC heated discharges is studied as a function of plasma shape, i.e. as a function of elongation $1.1 < \kappa < 2.15$ and triangularity $-0.65 \leq \delta \leq 0.5$. The electron energy confinement time is found to increase with elongation, in part due to the increase of plasma current with elongation. The beneficial effect of negative triangularities is most effective at low power and tends to reduce at the higher powers used.

The large variety of sawtooth types observed in TCV for different power deposition locations from on axis to the q=1 region can be simulated with a model including a local power deposition, a growing m/n=1 island (convection and reconnection), plasma rotation and finite heat diffusivity across flux surfaces.

1. INTRODUCTION

The improvement in tokamak performance over the last 25 years is not only due to the fact that tokamaks have grown in size, but is also a result of modifications of the basic tokamak concept. The evolution from circular to noncircular cross sections and, in particular, the vertical elongation of the plasma cross section κ allows for higher plasma current, since the maximum current scales as $I_p \sim (1+\kappa^2)/2$.

Increasing the plasma current offers two advantages. The first advantage is that the global energy confinement time increases with current, according to several widely used scaling laws [1, 2]. The second advantage is that vertically elongated and D-shaped cross sections allow much higher normalised pressures, i.e. β values, than circular ones [3, 4]. The β-limit, determined from numerical MHD stability analysis [4], $\beta(\%) = c_T I_p(\mathrm{MA})/[a(\mathrm{m})B(\mathrm{T})]$, scales with the plasma current I_p; a is the minor radius, B the toroidal magnetic field, and c_T is the Troyon factor, which is typically between 2.5 and 4.0, depending on the pressure and current profiles. The good agreement of ideal β-limit calculations in highly elongated plasmas with experiment [5, 6] strongly suggests to increase the design κ in ITER.

Electron Cyclotron Heating [7, 8] (ECH) experiments on TCV (achieved parameters: R=0.89m, a=0.25m, κ=2.58, $-0.7<\delta<0.9$, I_p=1MA, B=1.43T) are presently aimed at the study of the confinement properties of variably shaped plasmas. For these studies, an ECH power of 1.4 MW is injected at the second harmonic, 82.7GHz. This power level is already an order of magnitude larger than the Ohmic power during ECH, but represents only a third of the planned

total power (3MW at the second harmonic and 1.5MW at the third harmonic, 118 GHz). EC heating has been chosen for TCV, to cope with the large variety of plasma shapes. Each 0.5 MW gyrotron is connected to a steerable launcher, which can be moved during a tokamak discharge. A universal polariser is included in each transmission line to provide the polarisation needed at the plasma boundary for optimal power coupling.

A number of improvements have been made to the first wall graphite protection during the 1997 shutdown. Surface coverage has been increased from ~60% to ~90% by addition of new tiles on previously exposed areas on the low field side wall. These new elements now allow for heating of negative triangularity discharges. The central column tiles have been completely redesigned and have now a toroidal profile optimised for high power experiments. The wall is boronised regularly.

2. CONFINEMENT AS A FUNCTION OF PLASMA SHAPE

2.1 Confinement study: definition and parameter range

The aim is to study confinement as a function of elongation κ, ($1.1 < \kappa < 2.15$), and triangularity δ, ($-0.65<\delta<0.55$). Two values of q_{eng} ($q_{eng}=5abB/RI_p$), 1.7 and 3 are used, ($2.3<q_a<6$; $0.2<I_p<0.7$MA). The engineering safety factor q_{eng} is used instead of the usual q_a to parametrise the plasma current since constant q_{eng} results in similar normalised profiles independent of the plasma shape [9]. The standard central density n_{eo} is ~2-2.5×10^{19} m^{-3}, while the influence of density is only studied for a restricted number of shapes. All discharges are limited L-mode discharges. Up to 1.4 MW ECRH was injected, with the power deposition region located near the magnetic axis, largely inside the sawtooth inversion radius. At higher q_{eng}, due to finite beam width and shrinking of the q=1 surface, together with a smaller paramagnetic resonance shift at lower current, the beam moves somewhat off-axis, but is still well inside the q=1 radius. Thus, we have always central power deposition conditions.

Three gyrotrons were used for this study, two of them launching from the upper lateral ports and one from the equatorial port. The power was raised to its maximum value in three steps of typically 0.2 s duration. Confinement data are used after the establishment of a constant soft X-ray flux, which led to the exclusion of a 40-50 ms transient period at the start of each power step. Between the 2nd and 3rd step the power was modulated during 0.2 s. The power deposition location was obtained from soft X-rays at the EC shut-off, from power modulation experiments, and qualitatively from the sawtooth shapes (see section 3.1).

The EC power, P_{EC}, is measured near the torus calorimetrically between discharges. The gyrotron power can be set within 5% and is indeterminate to ±10%. The elliptical polarisation of the X2-beam is adjusted to maximise the power coupling at the plasma boundary for all geometries. In most of the cases studied, the power coupled to the X-mode was calculated as greater than 98%.

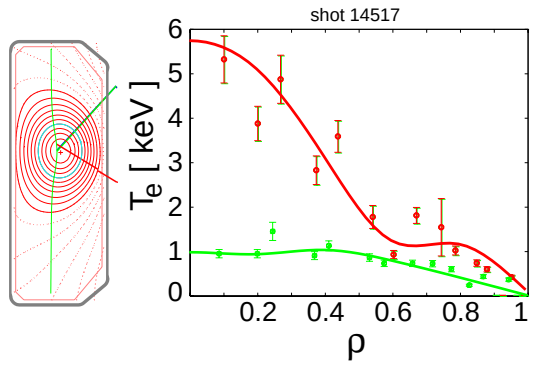

FIG. 1. Thomson electron temperature profile for κ=1.5, δ=0.2, $n_{eo}=1.3\times10^{19}m^{-3}$ during Ohmic and ECRH (1.4 MW). The central deposition aimed with upper lateral and equatorial launchers is indicated.

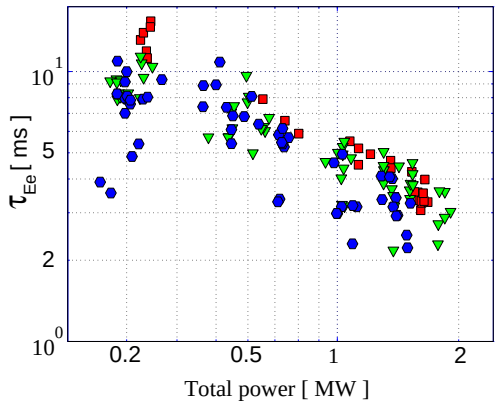

FIG. 2. Electron confinement time versus total power for κ=1.5, δ=0.2 (squares: $n_{eo19}>3$, triangles: $2<n_{eo19}<3$, hexagons: $n_{eo19}<2$).

The electron energy content W_{Ee} is obtained from Thomson scattering measurements, taken every 17 ms. The T_e and n_e profiles, measured along a vertical chord (at R=0.9m), are projected onto normalised flux co-ordinates and fitted with cubic splines. Therefore the calculation of W_{Ee} depends on the equilibrium reconstruction and on the profile fits. This procedure is straightforward for positive triangularity and low elongation discharges, where MHD mode activity is low. For negative triangularity and high elongation, the profiles show occasionally large fluctuations within the sawtooth inversion radius, which can make the fitting procedure problematic. Such shots were rejected from the database. The electron energy sometimes fluctuates strongly in time owing to large sawtooth relaxations at positive triangularity and with 1.5 MW of ECRH, as shown in Fig. 1. Typically ten Thomson profiles were available after the exclusion of the initial transient period at the beginning of each step. These multiple profiles were averaged to reduce the influence of fluctuations.

Typical values of the effective charge Z_{eff}, calculated from soft X-ray flux (dominated by carbon emission) and Thomson temperatures, are $Z_{eff} \geq 4$ during the Ohmic and ECRH phases. Ion temperatures from neutral particle analysis range from 200 to 250 eV. Therefore the ion contribution to the total energy is negligible.

2.2 MHD activity

MHD activity does not only influence the T_e profile reconstruction but can also degrade the confinement itself. In particular for $\delta < -0.2$ the m/n=2/1 mode has been frequently observed during phases with and without auxiliary heating power and irrespective of the edge safety factor.

Sawteeth were present in a wide range of the investigated plasma shapes. Ohmic sawteeth, at κ=1.5, δ=0.2 and typical densities of 2-3×10^{19}m^{-3} have a period $\tau_{ST} \sim 2$ ms. Their period and size increase with triangularity up to $\tau_{ST} \sim 3$ ms and up to a relative crash amplitude, observed with a soft X-ray diode viewing the plasma core (I_{SX-R}), of 20%. For negative δ the relative crash amplitude decreases down to a few % and can disappear within the resolution limit [10]. The crash amplitude as well as the sawtooth period decrease with elongation. Occasionally, no sawteeth have been observed in discharges with $\kappa > 2$.

With ECH deposition within the q=1 surface, different forms of sawteeth have been observed, ranging from normal triangular sawteeth for on-axis deposition to saturated and inverted sawteeth for deposition closer to the inversion radius. For q_{eng}=2, κ=1.55, δ=0.25, the observed sawtooth shapes change with increasing heating power from normal to saturated to inverted sawteeth. For higher q_{eng}=3, saturated sawteeth already appear at lower heating power, indicating that the actual deposition was somewhat off-axis (see section 3.1.1).

The effect of power on sawtooth period and size depends on triangularity: for instance at κ~1.5, for δ>0.2 and low q_{eng} to ensure central deposition, the sawtooth period and crash amplitude increase with increasing heating power up to $\tau_{ST} \sim 5$ ms and up to a relative crash amplitude of 35%, whereas for δ<0.2 the sawtooth period decreases with increasing heating power.

2.3 Scaling of electron energy confinement time

The dependence of the electron energy confinement time on total power and density was studied over a wide power range in the centre of the (κ,δ) scan (κ=1.5, δ=0.2), as shown in Fig. 2. The electron energy confinement time is clearly seen to decrease with power and to increase with density.

In an attempt to obtain a simple general power law to describe the dependence of τ_{Ee} on n_e, P, κ, δ and I_p, we have applied a multi-variable regression to the database. The dependences on κ and I_p cannot be separately determined, owing to the strong correlation between these quantities in our data set. The power law we are able to express so far must therefore contain a free parameter, as follows:

$$\tau_{Ee}[\mathrm{ms}] = 1.9 \times 6.5^{\alpha_I}\, n_{e\_av19}^{\alpha_n}\, P^{\alpha_P}\, I_p^{\alpha_I}\, \kappa^{\alpha_\kappa}\, (1+\delta)^{\alpha_\delta}\ [\mathrm{m}^{-3}, \mathrm{MW}, \mathrm{MA}], \qquad (1)$$

where α_n=0.45±0.2, α_P=-0.75±0.1, α_δ=-0.35±0.3, α_κ=1.5(1-α_I)±0.4 and α_I remains undetermined. These uncertainties result from a 25% error on τ_{Ee}. Good fits are obtained with α_I in the range $0 \leq \alpha_I \leq 0.7$, as illustrated in Fig. 3 for the case $\alpha_I = 0.5$.

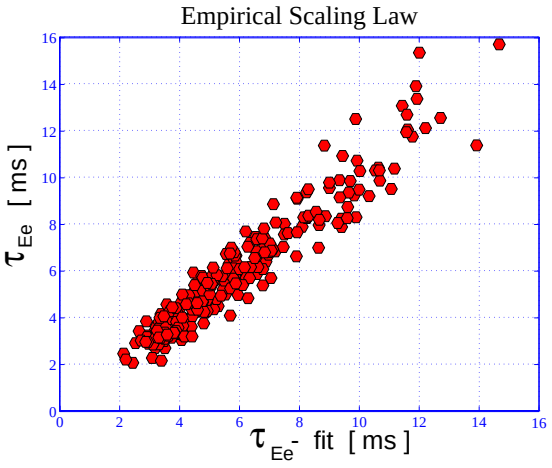

FIG. 3. Empirical scaling law for TCV ECRH data set, see equation (1).

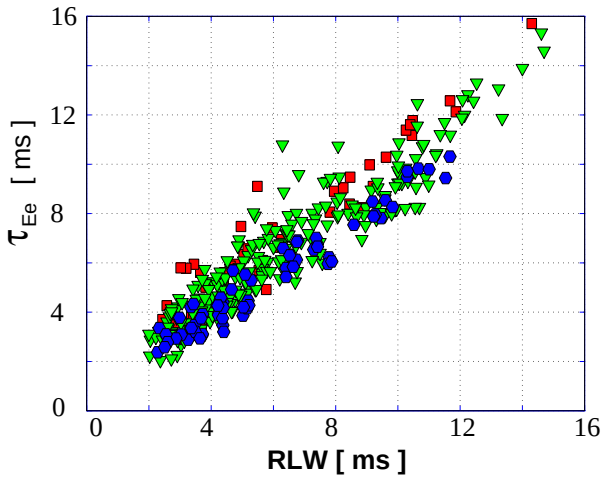

FIG. 4. Fit to Rebut-Lallia-Watkins scaling law. The triangularity is not in the RLW scaling. Negative δ appear favourable (squares: δ<0, triangles: 0<δ<0.3, hexagons: δ>0.3).

Naturally, such a general scaling, being based on the entire data set, may overlook more detailed effects in particular regions of the parameter space. For instance, power degradation can be calculated for each discharge separately, using the different power steps. This shows that the power degradation increases with density. Also, the beneficial effect of low triangularity or slightly negative triangularity appears to be stronger at low total power.

Most of the improvement with shape in Ohmic plasmas had been explained earlier in terms of geometrical effects. The thermal conductivity of ohmic plasmas was found to be independent of the shape. This observation, combined with geometrical effects on the temperature gradient and degradation with increasing energy flux, was able to explain the observed variation in the energy confinement time [11].

The TCV data is plotted against the Rebut-Lallia-Watkins confinement scaling [12] for comparison, in Fig. 4, and is seen to fit satisfactorily. Since the RLW scaling contains no triangularity dependence, the data points are subdivided in three triangularity classes, showing the beneficial effect of negative triangularity.

2.4 Transport modelling (PRETOR, ASTRA)

Some of the EC heated discharges have been simulated using the code PRETOR [13]. PRETOR is a predictive time-dependent transport simulation code for tokamaks: it couples a 2-D equilibrium solver with the flux-surface averaged 1-D transport equations to compute the evolution of temperature and density of electrons and ions. The RLW model [12], which is implemented in the code, has been modified, only in its geometrical dependence, to simulate discharges with an edge safety factor larger than 5, as the original model does not allow satisfactory simulations of Ohmic TCV discharges in this domain [14]. The experimental temperature profiles of a single shot in the ohmic phase have been analysed and the heat conductivity has been adjusted to reproduce the experimental behaviour, which implies a relatively large transport at the edge ($\chi_e(\rho=0.8)\sim 2 m^2/s$).

With this model, keeping fixed parameter values in all the transport coefficients, discharges have been simulated in the Ohmic and in the ECH phases. A satisfactory agreement is obtained for the temperature, Fig. 5, and density profiles, the electron thermal energy and confinement time, assuming total absorption for the different ECH powers injected.

Simulating the same discharge with ASTRA, a transport code based on the canonical transport model [15], a model of self-consistent profiles, good agreement is found with temperature profiles and confinement time. With a measured ratio of $P_{rad}/P_{OH}\sim 0.2$, using the radiated power measured from bolometry, one must assume only 90% absorption of injected power. A higher radiation level, around $P_{rad}/P_{OH}\sim 0.3$, would result in full power absorption. Thus our data can satisfactorily be simulated by both transport codes.

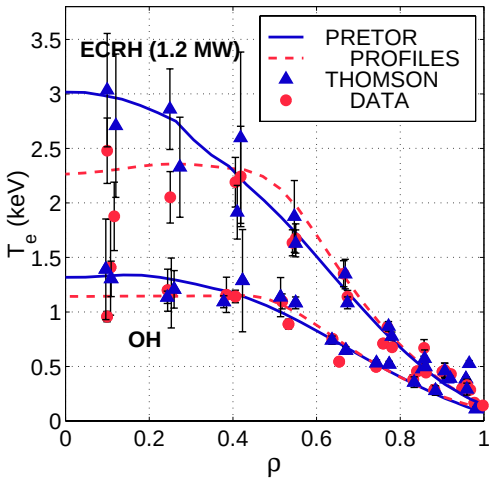

FIG. 5. Comparison between PRETOR temperature profiles and TCV experimental data in Ohmic and ECR heated (1.2 MW) discharges, before (solid line) and after (dashed) sawtooth crash (κ=1.8, δ=0.2, $n_{eo}=2.3\times10^{19}m^{-3}$, q~5).

3. SIMULATION OF CENTRAL RELAXATIONS WITH LOCALISED POWER DEPOSITION

3.1 Central relaxation shape modelling

3.1.1 Experimental description

Non-standard sawtooth traces have been observed in TCV during intense localised EC heating [16]. Fig. 6 shows a sequence of soft X-ray traces obtained while varying the ECH deposition radius. With on axis deposition, standard, i.e. triangular, sawteeth are observed. However, as the ECH absorption region is moved off-axis, the soft X-ray traces change their shape: partially saturated and saturated sawteeth are observed when the heating is still within the q=1 radius. Interestingly, the precursor oscillations that precede the fast relaxation phase of a saturated sawtooth sometimes double their frequency. Humpback sawteeth, first reported by the T-10 team [17], are observed in TCV when the heat is deposited close to the inversion radius. For slightly larger deposition radii, the soft X-ray traces acquire hill-like shapes of low amplitude. Another intriguing experimental observation concerns the optimal deposition radius for obtaining high central temperatures: this radius appears to be close to the q=1 radius. In fact, the sawtooth or humpback period is longest in this case, and the confinement time is at least as large as for central deposition.

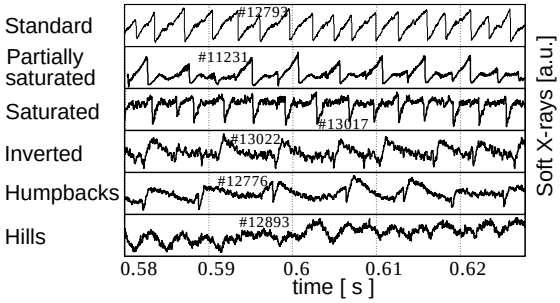

FIG. 6. Standard sequence of central relaxations. Standard sawteeth are produced by on axis power deposition, humpbacks and hills by deposition close to sawtooth inversion radius.

3.1.1 Model of a growing island under localised heating and diffusion

A theoretical model has been recently developed, which accounts for many of the observed features [18] as a function of the heating deposition region. The model is based on the combined effects of m/n=1 magnetic island dynamics, localised EC heating, finite heat diffusivity across the magnetic field lines and plasma rotation. According to this model, the flux surfaces acquire a distinct m/n=1 topology in the plasma central region. The thermal energy distributes uniformly on flux surfaces because of the large (practically infinite) parallel thermal conductivity. Rotation spreads the deposited heat on several flux tubes intersecting the ECH absorption region. Then, the temperature evolution is dominated by heating and perpendicular diffusion (a constant $\chi_\perp$ is assumed) in periods during which the m/n=1 island is either absent or has a stationary width, while convection and mixing due to reconnection become important when the island is growing, the

convection pattern being associated with the specific *m/n*=1 internal kink mode structure. The model was originally applied to explain the multi-peaked temperature profiles and transport barriers observed in high ECH power density experiments such as RTP [19] and TEXT-U [20]. In this paper, we present two examples which indicate the model ability to reproduce the observed sawtooth shapes in TCV.

In the first example, Fig. 7, a saturated sawtooth is simulated. In this simulation, the heating deposition region is assumed to be between about 2 cm and 4 cm from the equilibrium axis on the high field side; the *q*=1 radius is at 7 cm. Thus, the heating is off-axis, but is well within the *q*=1 radius, consistently with the experimental indications. Fig. 7a) shows the simulated temporal trace of the local electron temperature at a distance of about 2 cm from the equilibrium magnetic axis. In Fig. 7b), three temperature profiles at different phases of the saturated sawtooth are shown. These profiles are non-monotonic within the mixing radius, ρ_{mix} and can become rather spiky. In Fig. 7c), a simulated 3D reconstruction of the electron temperature corresponding to the fast relaxation phase at time $t = t_3$ of Fig. 7a) is shown.

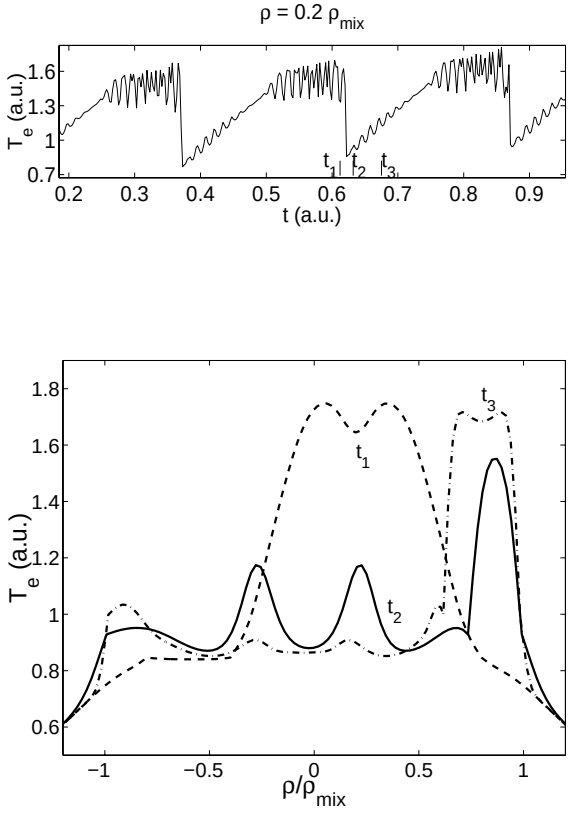

FIG. 7. Simulation of partially saturated sawteeth with power deposition between magnetic axis and the q=1 surface ($\rho=0.2\rho_{mix}$)
7a) temporal evolution of the central temperature. Note the appearance of frequency doubling,
7b) temperature profile before (t_1) and after crash (t_2 ,t_3), see fig. 7a),
7c) 3D temperature profile at time $t=t_3$, after crash.

In the second example, Fig. 8, we present the simulation of a humpback sawtooth. In order to obtain a humpback from our model, it is important to place the heating region close to the *q*=1 radius, consistently with the experiment. This produces slightly hollow temperature profiles during the quiescent phase, which then become peaked in the centre as a consequence of the growth of the *m*=1 island. Fig. 8a) shows the temporal evolution of the central electron temperature. Temperature profiles during the fast relaxation phase are shown in Fig. 8b). Note the relative minimum in the temperature, which deepens with time during the fast phase of the humpback relaxation. Indeed, the characteristic signature corresponding to the sudden drop in temperature between the two humps, visible in Fig. 8a), is related to the fast passage of this relative minimum through the observation point. A 3D reconstruction of the electron temperature is shown in Fig. 8c).

For both simulations, the island width, *w(t)* is assumed to grow rapidly during the observed, fast relaxation phase. More specifically, for the case of the simulated saturated sawtooth, *w(t)* grows from 0.4 ρ_{mix} to 1.6 ρ_{mix} in about 200 μs (corresponding to a radial displacement of the original magnetic axis between 0.2 ρ_{mix} and 0.8 ρ_{mix}); for the humpback sawtooth, *w(t)* grows from practically zero to 1.8 ρ_{mix} in a similar time interval. These values of *w(t)* are consistent with nearly full reconnection. This behaviour is not predicted theoretically, but it can be inferred from the

experimental data. Nevertheless, the model is applicable as well to cases of partial sawtooth reconnection. The typical radial width of the heat deposition region used in the simulations is between 1 and 2 cm. The results are not particularly sensitive to this width when it varies within this range.

Thus, the model successfully reproduces the shapes of different types of central relaxations as the heating radius is varied, at least qualitatively speaking. In addition, consistently with the experiments, the relative amplitude of the relaxations for central versus off-axis deposition comes out correctly. For example, at constant power injection, high amplitude triangular sawteeth are obtained for on-axis heating, while low amplitude humpback oscillations are obtained when the heating region is close to the q=1 surface.

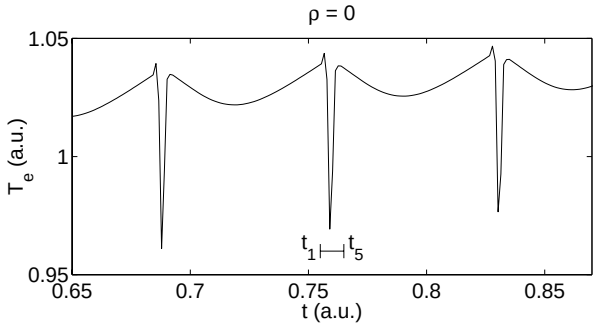

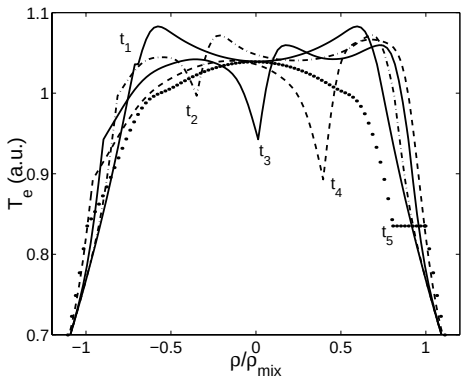

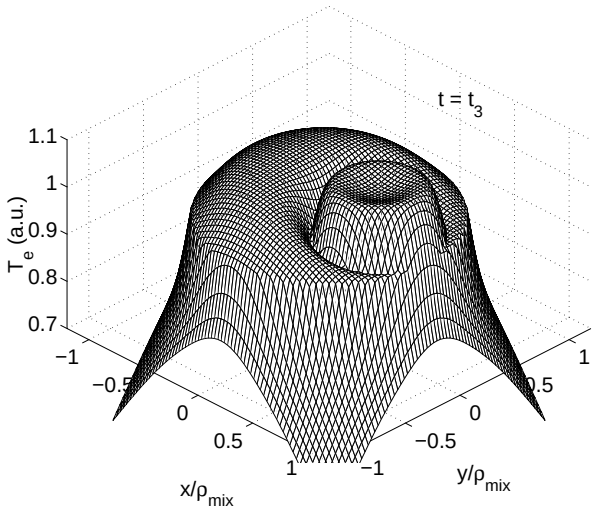

FIG. 8. Simulation of humpback sawteeth with power deposition close to q=1 surface:
8a) temporal evolution of the central temperature,
8b) temperature profile during the fast phase indicated in fig. 8a),
8c) 3D temperature profile in the middle of the crash ($t=t_3$)

3.2 Sawtooth period simulation with localised power deposition

The transport code PRETOR (see section 2.4), including a sawtooth model developed earlier [21], had been used earlier to simulate sawtooth periods in Ohmic discharges of TCV [22]. It is now used to simulate ECR heated discharges, since it is known that temperature and density profiles are strongly influenced by the presence (or absence) of sawteeth. In particular, the strong dependence of the sawtooth period on power deposition location observed experimentally can also be simulated.

The magnetic shear $s_1 = \rho_1 q'(\rho_1)/q_1$ at q=1 and $s_{1\mathrm{crit}}$, a critical shear above which the resistive internal kink is triggered, define the time at which the sawtooth crash occurs. The sawtooth period depends on the relative time evolution of s_1 and $s_{1\mathrm{crit}}$, and therefore mainly on the local plasma parameters. This explains why the sawtooth activity is very sensitive to ECRH as seen in TCV [16]. Indeed, local heating can change both $s_1(t)$, by changing the local resistive time and the current profile, and $s_{1\mathrm{crit}}(t)$ by changing the temperature gradients and confinement time. Moreover, localised deposition affects the q=1 radius both in the transport code and in the experiment, as revealed by measurements of the sawtooth inversion radius. We have simulated a case with 0.5 MW of ECRH deposited over a radial width of 0.15 a. Changing the mean deposition radius from ρ = 0 to 0.3 to 0.5, the code gives ρ_1/a = 0.44, 0.40 and 0.27 respectively. In addition, in the first two cases, $s_{1\mathrm{crit}}$ is relatively large, 0.35, because heating inside q=1 gives large gradients at q=1. Therefore long sawtooth periods are obtained, while heating outside ρ_1 gives a very small s_{1crit} and short sawtooth periods. This is in qualitative agreement with the experiment where

sawtooth periods of 2 ms are observed when heating outside q=1 and sawtooth periods increase rapidly to 7-8 ms when heating near the q=1 surface. However, heating closer to the magnetic axis results again in shorter sawtooth period; this indicates that a more detailed simulation including the magnetic topology described above, will be required.

4. CONCLUSIONS

The electron energy confinement has been studied as a function of plasma shape, i.e. as a function of elongation and triangularity in EC heated discharges, with P_{EC} exceeding P_{OH} by up to an order of magnitude. The electron energy confinement improves with elongation. The beneficial effect of low or negative triangularity on confinement, manifested in Ohmic plasmas, is also observed in EC heated plasmas, but tends to decrease with increasing power. Results of transport simulations, using two different models, are found to be consistent with the experimental data.

A variety of different types of central relaxations (sawteeth) are observed when the location of power deposition is moved from the magnetic axis to the q=1 region. The observed sawtooth shapes have been successfully simulated, using a model with localised power deposition, a growing (convection and reconnection) and rotating island at q=1, and finite thermal diffusivity across field lines. Sawtooth shapes similar to those observed in the experiment are reproduced when the power deposition location is moved from the magnetic axis to the q=1 region.

The observation that the sawtooth period is maximum when the power is deposited close to the q=1 surface has also been reproduced by simulation. The model simulates the evolution of the local magnetic shear and includes a critical shear above which the resistive internal kink is triggered.

5. ACKNOWLEDGEMENTS

This work was partly supported by the Fonds National Suisse de la Recherche Scientifique

REFERENCES

[1] CORDEY, J.G. et al., Plasma Phys. Controlled Fusion **39**, B115 (1997).
[2] MARTIN, Y. and SAUTER, O., Considerations on Energy Confinement Time Scalings using present Tokamak Databases and Prediction for ITER Size Experiments, Lausanne Report LRP 616/98.
[3] MILLER, R.L. et al., Phys. Rev. Lett. **43**, (1979) 765.
[4] TROYON, F. et al., Plasma Phys. Controlled Fusion **26**, (1984) 209.
[5] HOFMANN F. et al., Phys. Rev. Lett. **81**, 2918 (1998).
[6] LAZARUS E.A. et al., Phys. Fluids **B 3** (1991) 2220.
[7] GOODMAN T.P. et al., 19th Symp. on Fusion Technology, Lisbon, 1996, Vol I, 565.
[8] GOODMAN T.P. et al., presented by M.Q. TRAN. Invited Paper, 3rd Int. Workshop on Strong Microwaves in Plasmas, Russia, August 1996, ed. by A.G. Litvak, Nizhny Novgorod Univ. Press 1997.
[9] WEISEN H. et al., Plasma Phys. Control. Fusion **40** (1998) 1803.
[10] WEISEN H. et al., Nuclear Fusion **37** (1997) 1741.
[11] MORET, J-M., et al., Phys. Rev. Lett. **79** (1997) 2057.
[12] REBUT P.H., LALLIA P.P. and WATKINS M.L., Proc. 12th Int. Conf. Plasma Physics and Controlled Nuclear Fusion Research, Nice 1988, IAEA Vienna 1989, Vol. 2, 191.
[13] BOUCHER D. and REBUT P.H., in Proc. IAEA Tech. Com. on Advances in Simulation and model. of Thermonuclear plasmas, 1992, Montreal (1993) 142.
[14] ANGIONI C. et al., Proc. of Theory of Fusion Plasmas, Varenna 1998 and LRP 617/98.
[15] DNESTROVSKII Y.N. et al., Plasma Phys. Reports, **23** (1997), (transl. from Fizika Plazmy).
[16] PIETRZYK Z.A. et al., Proc. of Joint ICPP 1998 and 25th EPS, Praha 1998, and LRP 610/98, July 98.
[17] KISLOV D.A. et al., 22nd EPS Conf. on Contr. Fus. and Plasma Phys., Vol. 19C, Part I (1995) 369.
[18] PORCELLI F., ROSSI E. et al., Politecnico di Torino Report, Oct. 1998 PTDE/IN, subm. for publication.
[19] LOPES CARDOZO N.J. et al., Phys. Rev. Lett. **73**, (1994) 256.
[20] CIMA G. et al., Plasma Physics and Controlled Fusion **40** (1998) 1149.
[21] PORCELLI F. et al. Plasma Phys. Contr. Fusion **38** (1996) 2163.
[22] SAUTER O., ANGIONI C. et al., Proc. of Theory of Fusion Plasmas, Varenna 1998 and LRP 617/98.